Improvement in carrier mobility and photovoltaic performance through random distribution of segments of linear and branched side chains†

Daniel A. M. Egbe,*[a] Getachew Adam,[a] Almantas Pivrikas,[a] Alberto M. Ramil,[a] Eckhard Birckner,[b] Vera Cimrova,[c] Harald Hoppe[d] and Niyazi Serdar Sariciftci[a]

Received 17th May 2010, Accepted 21st June 2010
DOI: 10.1039/c0jm01482f

The random distribution of segments of *linear* octyloxy side chains and of *branched* 2-ethylhexyloxy side chains, on the backbone of anthracene containing poly(*p*-phenylene-ethynylene)-*alt*-poly-(*p*-phenylene-vinylene) (PPE-PPV) has resulted in a side chain based statistical copolymer, denoted **AnE-PV*stat***, showing optimized features as compared to the well defined homologues whose constitutional units are incorporated into its backbone. Electric field independent charge carrier mobility (μ_{hole}) for **AnE-PV*stat*** was demonstrated by CELIV and OFET measurements, both methods resulting in similar μ_{hole} values of up to 5.43×10^{-4} cm^2 V^{-1} s^{-1}. Upon comparison, our results show that charge carrier mobility as measured by CELIV technique is predominantly an *intra*chain process and less an *inter*chain one, which is in line with past photoconductivity results from PPE-PPV based materials. The present side chain distribution favors efficient solar cell active layer phase separation. As a result, a smaller amount of $PC_{60}BM$ is needed to achieve relatively high energy conversion efficiencies above 3%. The efficiency of $\eta_{AM1.5} \approx 3.8\%$ obtained for **AnE-PV*stat***:$PC_{60}BM$ blend is presently the state-of-art value for PPV-based materials.

Introduction

Conjugated compounds have proven their potential for the design of organic photovoltaic (OPV) devices as low cost energy sources.[1–5] Intensive interdisciplinary research in this area is presently going on worldwide and results in a rapid enhancement of the state-of-art power conversion efficiency, $\eta_{AM1.5}$. Certified $\eta_{AM1.5}$ values above 6% have been reported for polymer based OPVs.[6,7] First products based on OPV are now marketed.[8] The bulk heterojunction concept consisting of an intermixing of the donor and acceptor components in the active layer has proven to be the most efficient way to design high performance devices. The way both components intermix is crucial for the overall performance of the solar cells. There are different approaches followed on how to favorably tune the nanoscale morphology of the donor and acceptor blend.[9,10]

We have recently shown that the hydrophobic nature of solubilizing alkoxy side chains can be utilized to tune the active layer blend morphology of PPE-PPV:fullerene bulk heterojunctions by variation of the side chain volume fraction.[11] We furthermore demonstrated that linear and branched alkoxy side groups and combinations thereof can be used to tune the backbone π–π-stacking distance, $d_{\pi-\pi}$, and the interlayer separation, d_{inter} of anthracene-containing PPE-PPVs.[12,13] For instance all octyloxy substitution as in **AnE-PV*aa*** (for chemical structures see Chart 1) results in an insoluble polymer that exhibits a well organized layered structure.[13] Exchanging the linear octyloxy side chains in part by branched 2-ethylhexyloxy side chains at the phenylene-vinylene segment as in **AnE-PV*ab*** yields a soluble but less organized polymer with improved solar cell performance in terms of power conversion efficiency ($\eta \approx 2.4\%$) from a **AnE-PV*ab***:PCBM (1 : 1) blend, compared to

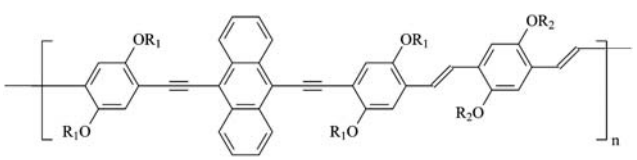

AnE-PV*aa*: $R_1 = R_2$ = octyl
AnE-PV*ad*: R_1 = octyl, R_2 = decyl
AnE-PV*ab*: R_1 = octyl, R_2 = 2-ethylhexyl
AnE-PV*ba*: R_1 = 2-ethylhexyl, R_2 = octyl
AnE-PV*bb*: $R_1 = R_2$ = 2-ethylhexyl

Chart 1 Chemical structures of already reported polymers **AnE-PV**.[12b] The constitutional units of **AnE-PV*aa***, ***-ab***, ***-ba*** and ***-bb*** are incorporated in **AnE-PV*stat***.

[a]*Linz Institute for Organic Solar Cells (LIOS), Johannes Kepler University Linz, Altenbergerstr. 69, 4040 Linz, Austria. E-mail: daniel_ayuk_mbi.egbe@jku.at; Fax: +43-2468-8770; Tel: +43-732-2468-8398*
[b]*Institute of Physical Chemistry, Friedrich-Schiller University Jena, Lessingstr. 10, 07743 Jena, Germany*
[c]*Institute of Macromolecular Chemistry, Academy of Sciences of the Czech Republic, Heyrovský Sq. 2, 162 06 Prague 6, Czech Republic*
[d]*Institute of Physics and Institute of Micro- and Nanotechnologies, Ilmenau University of Technology, Weimarer-Str. 32, 98693 Ilmenau, Germany*

† Electronic supplementary information (ESI) available: The experimental section describing the synthesis and characterization of the polymer as well the various experimental techniques, the cyclic voltammogram of **AnE-PV*stat***, *I–V* curves of 1 : 1 and 1 : 3 **AnE-PV*stat***:PCBM blend together with their corresponding IPCEs and AFM images of the active layers (thicker films), and *I–V* curves of 1 : 1 and 1 : 2 **AnE-PV*stat***:PCBM blend (thinner films) are provided. See DOI: 10.1039/c0jm01482f

its all-linear substituted but higher side chain volume fraction counterpart **AnE-PV*ad*** ($\eta \approx 1.5\%$).[12] The grafting of predominantly bulky branched 2-ethylhexyloxy as in **AnE-PV*ba*** and ***-bb*** leads to amorphous materials, whose 1 : 1 polymer:PCBM blend exhibit even lower photovoltaic performance ($\eta \approx 0.3$–0.5%).

In order to obtain a balanced material with optimized parameters, *i.e.* high solubility, similar side chain density as in **AnE-PV*aa***, ***-ab***, ***-ba*** and ***-bb***, and well organized supramolecular arrangement, a side chain based statistical copolymer, **AnE-PV*stat***, has been synthesized. This polymer comprises segments of linear octyloxy and segments of branched 2-ethylhexyloxy side chains that are evenly distributed along the conjugated backbone in a random manner. As such it combines the building units of its all linear (**AnE-PV*aa***), linear as well as branched (**AnE-PV*ab*** and ***-ba***), and all branched (**AnE-PV*bb***) constitutionally well defined counterparts.

To the best of our knowledge, a solely alkoxy side chain based statistical conjugated copolymer, purposely designed for solar cell active layer morphology control is not known. Alkoxy side chain based statistical conjugated copolymers have been designed for sensory[14] and for OFET (organic field effect) applications.[15] All conjugated diblock copolymers poly-(3-hexylthiophene)-*block*-poly(3-(2-ethylhexyl)thiophene)s (P(3HT)-*b*-P(3EHT)) making use of two different alkyl side chains were recently synthesized by *Hashimoto et al.* for opto-electronic applications.[16]

In this article, we describe the properties (photophysical, charge carrier mobility and photovoltaic) of **AnE-PV*stat*** and compare them with those of the well defined homologues **AnE-PV*aa***, ***-ab***, ***-ba*** and ***-bb***. Charge carrier mobility was measured based on both CELIV (Charge Extraction by Linearly Increasing Voltage) and OFET (Organic Field Effect Transistor) techniques.

Results and discussion

(A) Synthesis and general characterization

Synthesis and structural characterization. The side chain based statistical copolymer **AnE-PV*stat*** was obtained in 89% yield after reacting equimolar ratios of two dialdehydes **1a** (C_8H_{17} = octyl) and **1b** (C_8H_{17} = 2-ethylhexyl) with two bisphosphonate esters **2a** (C_8H_{17} = octyl) and **2b** (C_8H_{17} = 2-ethylhexyl) as illustrated in Scheme 1. The chemical structure was elucidated by NMR, IR and elemental analysis. GPC (gel permeation chromatography) measurements revealed a number-average-molecular-weight of $M_n = 28\,000$ g mol^{-1} with a PDI (polydispersity index) of 2.0 and a P_n (degree of polymerization) of 22. **AnE-PV*stat*** incorporates the repeating units of polymers **AnE-PV*aa***, ***-ab***, ***-ba*** and ***-bb***, whose chemical structures are shown in Chart 1. Their properties determined from GPC, TGA (thermogravimetric analysis) and WAXS (wide angle X-ray scattering) together with those of **AnE-PV*stat*** are summarized in Table 1 for comparison purposes.[12,13]

As expected, there is an increase of the π–π-stacking distance going from the solely linear octyloxy-substituted **AnE-PV*aa*** (0.380 nm) through **AnE-PV*ab*** (0.386 nm) having four-fold *linear octyloxy* and two-fold *branched 2-ethylhexyloxy* substitutions, to **AnE-PV*stat*** (0.393 nm).[13] **AnE-PV*stat*** exhibits, however, slightly higher degree of order in its self-assembly state than **AnE-PV*aa***, although its backbone incorporates segments decorated with branched side chains.[13] A similar observation was made with P(3HT)-*b*-P(3EHT), which was evidenced by higher structuring of its thin film absorption spectrum as compared to pure P3HT.[16]

The values displayed in Table 1 allow a comparison of the properties (photophysical, charge carrier mobility and photovoltaic) of **AnE-PV*stat*** with those of **AnE-PV*ab***, ***-ba*** and ***-bb*** because other influential parameters such as side chain volume fraction, molecular-weight distribution, solubility and purity of the various polymers are either the same or do not differ very much.

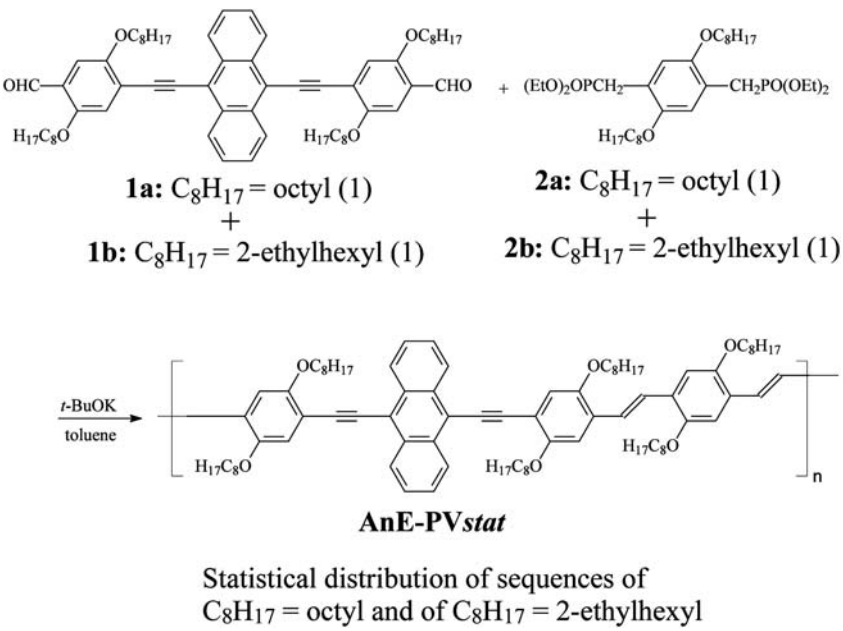

Scheme 1 Synthesis of side chain based statistical copolymer **AnE-PV*stat***.

Table 1 GPC (THF as eluent, polystyrene standards), TGA and WAXS results of the polymers **AnE-PV**: M_n = number-average molecular weight, PDI = polydispersity index, DP = degree of polymerization, $T_{5\%,10\%}$ = decomposition temperatures at 5% and 10% weight loss, respectively, and $d_{\pi-\pi}$ = π–π-stacking distance[12,13]

Polymer **AnE-PV*i***	M_n/g mol^{-1}	PDI	DP	$T_{5\%}$/°C	$T_{10\%}$/°C	$d_{\pi-\pi}$/nm
aa	—	—	—	326	343	0.380 ± 0.002
ad	19 000	2.7	15	306	317	0.380 ± 0.002
ab	40 000	3.5	32	330	351	0.386 ± 0.002
ba	26 000	3.0	20	327	348	—
bb	16 000	2.9	13	325	346	—
stat	28 000	2.0	22	312	322	0.393 ± 0.002

Table 2 Photophysical data in dilute chlorobenzene solution and in thin film spin cast from chlorobenzene

Polymer **AnE-PV*i***	λ_a/nm	$\lambda_{10\%}$ /nm	E_g^{opt} /eV	λ_f/nm	$\Delta\nu_{af}$ /cm^{-1}	Φ_f (%)	τ/ns	k_f/ns^{-1}	k_{nr}/ns^{-1}
Solution properties									
ab	553	590	2.10	585	990	57	0.94	0.61	0.46
stat	555	590	2.09	585	920	52	0.87	0.60	0.55
ba	510	578	2.15	583	2500	29	0.72	0.40	0.99
bb	522	582	2.13	583	3200	48	0.85	0.56	0.61
Thin film properties									
ab	508, 583	687	1.80	624	1100	2	—	—	—
stat	509, 582	652	1.90	620	1050	2	—	—	—
ba	504	636	1.95	605	3300	3	—	–	—
bb	527	613	2.02	600	2300	6	—	—	—

Photophysical and electrochemical studies. Dilute chlorobenzene solution and thin film photophysical data of **AnE-PV*stat*** in comparison with those of **AnE-PV*ab***, ***-ba*** and ***-bb*** are provided in Table 2, namely the absorption maximum λ_a, 10% of the absorption maximum from the lower energy edge, $\lambda_{a10\%}$, the optical band gap energy, E_g^{opt}, calculated using $1240/\lambda_{a10\%}$, the emission maximum λ_f, the Stokes shift, $\Delta\nu_{af}$, the fluorescence quantum yield, Φ_f (relative to rhodamine G6 in solution and absolute values from integrating sphere for thin films),[12b] the fluorescence lifetime, τ, the fluorescence rate constant, k_f, and the rate constant, k_{nr}, of radiationless deactivation.

Fig. 1 depicts the absorption, excitation and emission spectra in dilute chlorobenzene solution of **AnE-PV*ab***, ***-ba***, ***-bb*** and ***-stat***. Thin film absorption spectra of the four polymers are displayed in Fig. 2 (left) while both thin film absorption and emission spectra of **AnE-PV*stat*** are depicted in Fig. 2 (right).

Small deviations between the absorption and the excitation spectra in solution were observed. This gives an indication of small amounts of non-fluorescent species. However, the identical emission and excitation spectra measured at different excitation and emission wavelengths, respectively, are a strong evidence of only one emitting species in the polymers.

Already in solution, there are differences in the absorption band shapes between the amorphous polymers **AnE-PV*ba***, ***-bb*** and the polymers showing stacking behavior **AnE-PV*ab*** and ***-stat***. While the first group is characterized by a structureless main absorption band peaked at 510 nm and 522 nm, respectively, the second group exhibits red-shifted main absorption bands, which consist of a peak around 555 nm and a higher energy shoulder around 520 nm. This difference becomes even

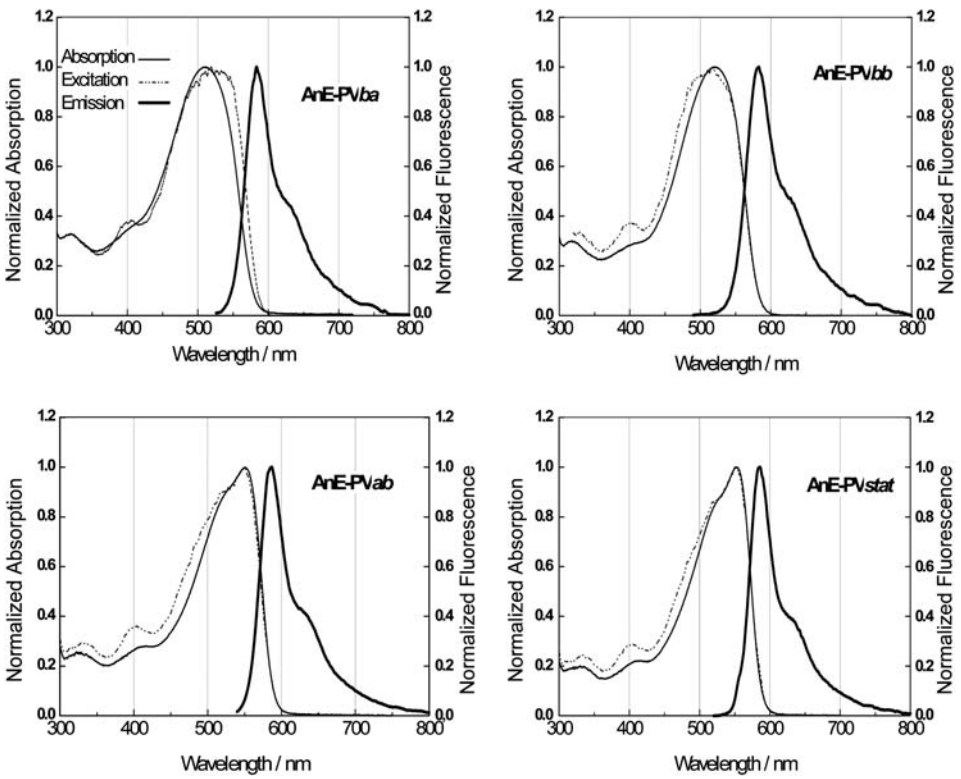

Fig. 1 Normalized absorption, excitation and emission spectra in chlorobenzene solution of **AnE-PV*ab***, ***-ba***, ***-bb*** and ***-stat***.

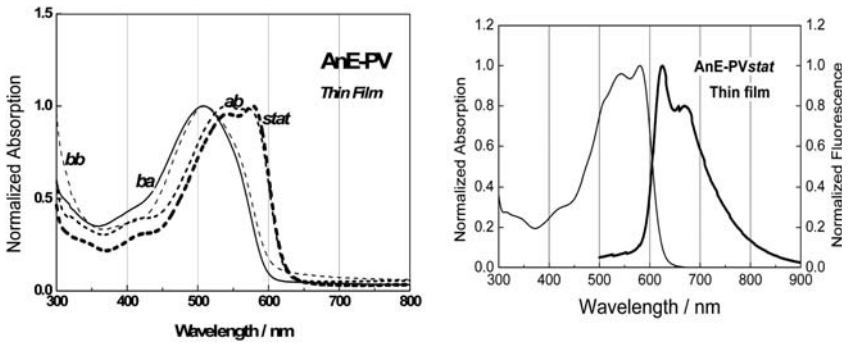

Fig. 2 (Left) Normalized thin film absorption spectra of **AnE-PV*ab***, **-*ba***, **-*bb*** and **-*stat*** (thin film spin-cast from $CHCl_3$ solution). (Right) Normalized thin film absorption and emission spectra of **AnE-PV*stat*** (thin film spin-cast from chlorobenzene solution). The data from chlorobenzene solution for **AnE-PV*ab***, **-*ba*** and **-*bb*** have been reported in ref. 12*b*.

clearer in thin film, whereby **AnE-PV*ab***[12b] and **AnE-PV*stat*** exhibit two well defined peaks around 510 nm and 580 nm *due to stacking* (layered structures), while **AnE-PV*ab*** and **-*bb***[12b] remain structureless. The slightly higher solution fluorescence quantum yields for both **AnE-PV*ab*** (57%) and **AnE-PV*stat*** (52%) and lower Stokes shifts, $\Delta\nu_{af}$, as compared to the amorphous polymers suggest a more planarized ground state. Moreover, **AnE-PV*stat*** shows the smallest Stokes shift both in solution and in thin film, which is an indication of comparatively less conformational changes from the ground to the first excited state, confirming its relatively conformationally stable nature.

All four polymers show identical solution fluorescence spectra peaked around 583 nm. From fluorescence kinetics measurements, a fluorescence lifetime $\tau = 0.87$ ns was obtained for **AnE-PV*stat***, which led to a fluorescence rate constant, k_f, of 0.60 ns^{-1} and a radiationless deactivation constant, k_{nr}, of 0.55 ns^{-1}. These values are similar to those of its well-defined homologues **AnE-PV*ab***, **-*ba*** and **-*bb***. In contrast, the thin film emission spectra of both **AnE-PV*ab***[12] and **-*stat*** are red-shifted and demonstrate more pronounced features due to aggregates as compared to the amorphous counterparts[12b] (Table 2 and Fig. 2, right). However, higher absolute fluorescence quantum yields were obtained for the amorphous materials due to less quenching channels as a result of fewer aggregations.[12b]

Electrochemical studies were carried out under identical experimental conditions as described in ref. 12*b* and 17. Representative cyclovoltammograms for scan rates of 20 and 50 m V^{-1} s^{-1} are displayed in Fig. S1†. HOMO and LUMO levels of 5.09 eV and 3.04 eV, respectively, were obtained for**AnE-PV*stat***. This results in an electrochemical band gap of $E_g^{elc} = 2.05$ eV which is in a good agreement with the optical band gap, E_g^{opt}, of 2.10 eV and 1.90 eV evaluated from the absorption edge of the solution and thin film spectra, respectively.[17]

(B) Charge transport studies

Charge transport studies were carried out using both CELIV and OFET techniques.

CELIV allows a direct measurement of the dispersive (time-dependent) charge carrier transport and recombination in films with energetical and structural disorder,[18–22] where time-resolved techniques like Time-of-Flight are not applicable.[23–25]

Dark CELIV current transient responses for different applied rising voltage pulses in **AnE-PV*stat*** polymer are shown in Fig. 3 (left). The studied films contain non-negligible thermally generated charge carrier concentration, therefore carrier photogeneration using a laser was not necessary.[26] A typical shift of an extraction maximum towards shorter times is seen when the applied voltage is increased. This demonstrates faster carrier extraction at higher applied electric fields, which allows drift velocity and mobility to be estimated as a function of applied electric field. Using equations derived elsewhere[18] and extraction maximum for each current transient shown in Fig. 3 (left),

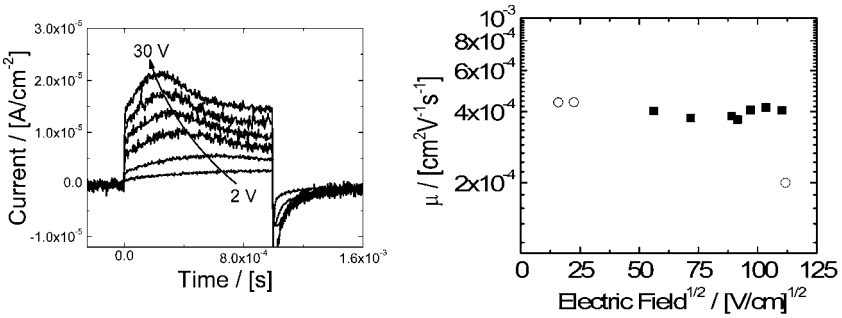

Fig. 3 (Left) Dark current extraction transients shown for different applied voltages in CELIV measurements of **AnE-PV*stat***. Left-shift of extraction maxima at higher applied voltages indicates faster carrier extraction time from which carrier mobility is calculated. (Right) The electric field independent charge carrier mobility at equilibrium in **AnE-PV*stat***. The closed squares represent carrier mobility from CELIV, whereas open circles show carrier mobility measured from OFET (see OFET section).

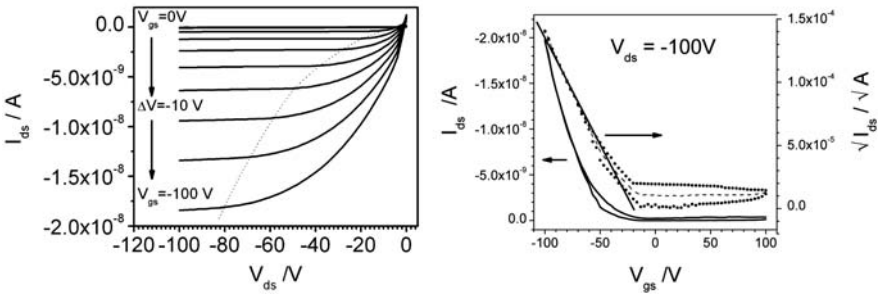

Fig. 4 (Left) Output characteristic of an **AnE-PV*stat*** OFET. The dotted line is placed in order to guide the eyes to the condition $V_{ds} \geq V_{gs} - V_{th}$, for which I_{ds} saturates. (Right) Left axis: transfer curve of an **AnE-PV*stat*** OFET, for a fixed $V_{ds} = -100$ V. Right axis: square root of I_{ds} (dotted line), mean value of the square root of I_{ds} (dashed line), and the linear fit to the mean value of the square root of I_{ds} (straight full line).

the equilibrium carrier mobility at different applied electric fields is calculated and plotted in Fig. 3 (right).[27] Film conductivity $\sigma = 2.6 \times 10^{-8}$ S cm^{-1} and mobile carrier concentration $n = 4 \times 10^{14}$ cm^{-3} due to the unintentional doping were directly estimated from the current extraction transients using equations derived elsewhere.[18] It was found that the conductivity was almost independent of the applied voltage in the measurement range.

AnE-PV*stat* OFETs were fabricated and electrically characterized. The field effect mobility was calculated in the saturation and linear regimes.[28–30] As observed in the output curve of an **AnE-PV*stat*** OFET presented in Fig. 4, the dependence of I_{ds} *versus* V_{gs} is characterized by a pinch off point afterwards I_{ds} saturates for values of $V_{ds} \geq V_{gs} - V_{th}$, ($V_{th}$ is the threshold voltage). The conductivity of the semiconductor **AnE-PV*stat*** was estimated to be 1×10^{-8} S cm^{-1}. It was calculated from the slope of the I_{ds} curve evaluated at $V_{ds} \cong 0$ V and $V_{gs} = 0$ V. The charge carrier density, n, in the OFET channel was estimated assuming 3 nm as the thickness of the layer within the semiconductor containing the electrical charges.[31] Hence, for $V_{gs} = -100$ V and $V_{th} = -20$ V a hole density equal to $n_h \approx 2 \times 10^{18}$ cm^{-3} was found. The field effect mobility in the linear regime was calculated from the slope, at very small V_{ds}, of the output curve corresponding to $V_{gs} = -100$ V of Fig. 5.[32,33] Hence, a constant field effect mobility of 4.4×10^{-4} cm^2 V^{-1} s^{-1} was obtained for V_{ds} equal to -2 and -4 V, respectively, which is similar to the ones obtained by the CELIV technique.

The calculation of the mobility in the saturation regime was done following the method of fitting the square root of I_{ds} as a function of V_{gs} to a straight line.[28,29,31,34] In the present case (see Fig. 4), due to the presence of a small hysteresis, it was preferred to work with the curve of the mean value of the square root of I_{ds} (dashed line) and to realize a linear fit to it (straight full line). The extracted charge carrier mobility and threshold voltage are equal to 2.0×10^{-4} cm^2 V^{-1} s^{-1} and -20 V, respectively. In addition, the device shows an on/off current ratio of $\sim$50. This value was calculated from the transfer curve as the ratio of I_{ds} at $V_{gs} = -100$ V and I_{ds} at V_{th}.

When evaluating carrier mobility values obtained from different methods, it is important to compare the electric field and carrier concentration at which the mobility has been measured. Therefore, the obtained values of the field effect mobilities are plotted, open circles, as a function of square root of the electric field in Fig. 3 (right). The values of the mobility shown in the range of the electric field from 15 to 25 (V/cm)$^{1/2}$ correspond to those calculated in the linear regime, low V_{ds} voltages. On the other hand, the point located around 110 (V/cm)$^{1/2}$ was calculated in the saturation regime, $V_{ds} = -100$ V.

The results from OFET and CELIV measurements show that, in the studied **AnE-PV*stat*** films, similar intrinsic film

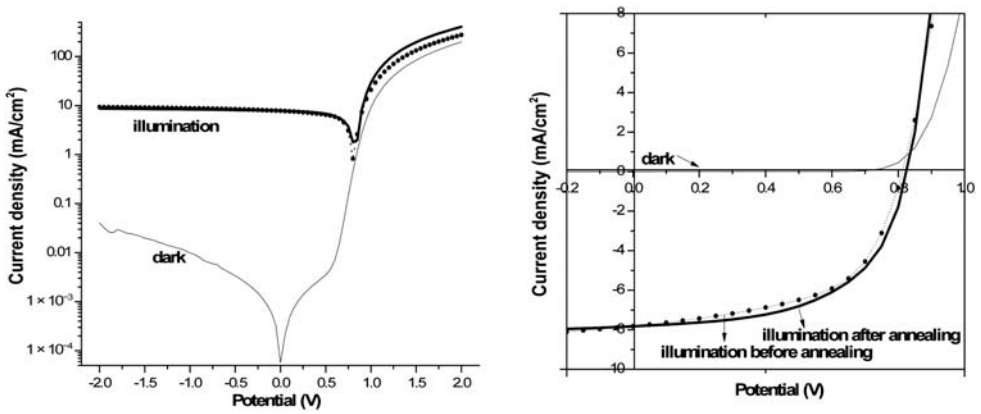

Fig. 5 Current–voltage (I–V) characteristics of the best solar cell from 1 : 2 ratio **AnE-PV*stat***:PCBM blend measured before and after annealing at 110 °C for 5 minutes.

Table 3 Hole mobility, μ_{hole}, of the polymers in increasing order

Sample	$d_{\pi-\pi}$/nm	μ_{hole}/cm^2 V^{-1} s^{-1}
AnE-PV*ad*	0.380 ± 0.002	1.7×10^{-5}
AnE-PV*ab*	0.386 ± 0.002	2.6×10^{-5}
AnE-PV*ba*	—	1.5×10^{-4}
AnE-PV*bb*	—	4.5×10^{-4}
AnE-PV*stat*	0.393 ± 0.002	5.4×10^{-4}

conductivity values and electric field independent charge carrier mobility were obtained (Fig. 3). The absence of electric field dependence and rather high carrier mobility indicates that no activation energy is required to reach higher mobility values. This provides a hint for the existence of optimal Density-of-States (DOS) for charge carrier transport in the studied **AnE-PV*stat*** polymer.[27,35] The charge carrier mobility will mainly depend on the concentration of charge carriers, as well as on the properties of DOS distribution.[36] Usually, higher charge carrier mobility values are reported for planar field effect transistor structures compared to diode geometry. As it has been observed before, in OFETs with low polarity dielectric, the measured mobility was very similar to the bulk mobility measured by TOF[37] suggesting that the DOS might have the same properties in the bulk of the material and at the interface. Even though in our experiments the charge carrier mobilities were measured at different carrier concentrations ($n = 4 \times 10^{14}$ cm^{-3} from CELIV and $n = 2 \times 10^{18}$ cm^{-3} from OFET), observed similar mobility values can be explained by the presence of narrow distribution of DOS. Such beneficial DOS for charge transport requires little activation energies and will render a charge carrier concentration and electric field independent mobility as observed from CELIV (Fig. 3).[35]

Obtained mobility values are the highest compared to the whole family group of anthracene based **AnE-PV** as well as poly[2-methoxy-5-(3,7-dimethyloctyloxy)phenylene-vinylene] (**MDMO-PPV**) polymers studied in the past (Table 3);[12,36] and is of the same order of magnitude (10^{-4}) as the polymers exhibiting the present state-of-art reported and certified energy conversion efficiencies of ~7%.[6] The mobility values are, however, close to those of the amorphous materials **AnE-PV*ba*** and **-*bb***, *i.e.* showing less stacking behavior.

It is ascertained from the data in Table 3 that intrinsic hole mobility as measured by the CELIV technique is favored by both *less stacking* (*i.e.* high $d_{\pi-\pi}$ values or no stacking at all). This leads to the conclusion that, at least for PPE-PPV type of materials, charge carrier mobility strongly follows an *intra*molecular path and less an *inter*molecular one. This agrees well with our past findings on photoconductivity studies carried out with PPE-PPVs, whereby high photocurrents were measured at low threshold voltages for polymers with less stacking tendency (due to grafting of a high number of bulky branched 2-ethylhexyloxy and/or long linear octadecyloxy side chains). It was then concluded that photoconductivity is more an *intra*molecular process than an *inter*molecular one.[38] Our conclusions are moreover supported by recent molecular dynamics (MD) simulations on charge mobility and transport mechanism of self-assembled P3HT molecules.[39] The authors used a hopping transport model to examine the variation of charge mobility with torsional angle and the π–π-stacking distance $d_{\pi-\pi}$ between two adjacent thiophene segments. The MD results indicated that the resultant mobility along the π–π *inter*-chain direction is significantly less than that along the *intra*-chain direction. Accordingly the main charge transfer route within P3HT ordered domains is an *intra*molecular rather than an *inter*molecular one.[39] van Breemen *et al.* also observed a significant improvement of OFET mobility up to 10^{-2} cm^2 V^{-1} s^{-1} *upon dilution* of the PPV backbone with both long linear undecanyloxy and octadecyloxy side chains.[15]

The observed electric field and concentration independent carrier mobility suggest the suitability of **AnE-PV*stat*** for applications as a hole transporting material or for use in high power conversion efficiency organic solar cells.

(C) Photovoltaic studies

Photovoltaic (PV) studies were carried out with 1 : 1, 1 : 2 and 1 : 3 **AnE-PV*stat***:PCBM blends. PV parameters were measured before and after annealing at 110 °C for 5 minutes. The nanomorphology of the various blends was also investigated before and after annealing using atomic force microscopy (AFM).

Fig. 5, S2 and S3† depict the *I–V* curves of 1 : 2, 1 : 1 and 1 : 3 **AnE-PV*stat***:PCBM ratios, respectively. It is ascertained from these curves that in dark condition the solar cells show a rectification ratio of approximately 10^4 at ±2V, an indication of efficient polarization of the device in the forward direction where electrons are injected from a low work function electrode (Al) to the LUMO of the blend while holes are injected from a high work function electrode to the HOMO of the blend. This is evidence of a good forward biased diode (solar cell).[40]

Irrespective of **AnE-PV*stat***:PCBM blend ratio, the solar cells showed reproducible open circuit voltage V_{OC} values between 800 and 840 mV which is a function of the HOMO of the polymer and that of the LUMO of the acceptor independent of the blend ratio.[2,41] The short circuit current J_{SC} and fill factor FF values were found to be dependent on both polymer:PCBM ratio and thermal treatment. As can be seen in Fig. 5 and S2 and S3† as well as Table 4, the short circuit current decreases with increasing PCBM proportion prior to annealing. After annealing at 110 °C, J_{SC} decreases in the case of the 1 : 1 blend ratio, remains almost

Table 4 Photovoltaic parameters from solar cells with different blend ratios of **AnE-PV*stat***:PCBM measured before (a) and after (b) annealing at 110 °C for 5 minutes. The active layer thickness was ~190 nm for 1 : 1 and ~245 nm for 1 : 2 and 1 : 3 blend ratios. Consistency of the results is demonstrated

		V_{OC}/mV		J_{SC}/mA cm^{-2}		FF (%)		η (%)	
Blend ratio	Sample no.	(a)	(b)	(a)	(b)	(a)	(b)	(a)	(b)
1 : 1	1	800	750	8.0	7.6	50	49	3.20	2.80
	2	815	750	7.6	7.3	52	45	3.21	2.47
	3	815	750	8.1	7.7	53	47	3.47	2.72
1 : 2	1	810	830	7.8	7.8	56	58	3.55	3.77
	2	820	820	6.1	7.1	47	59	2.36	3.45
	3	800	820	6.1	7.1	49	59	2.40	3.43
1 : 3	1	830	830	5.6	6.1	57	56	2.63	2.83
	2	840	820	5.5	6.4	52	58	2.40	3.05
	3	830	820	6.2	7.4	50	60	2.56	3.62

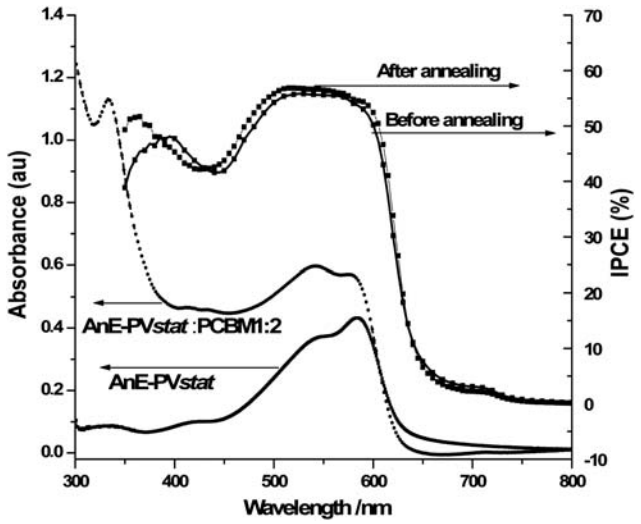

Fig. 6 IPCE curves of the best solar cells made from **AnE-PV*stat***:PCBM (1 : 2) blend before and after annealing at 110 °C for 5 minutes as well as the corresponding optical absorptions of the pristine polymer and the blend.

the same in the 1 : 2 blend ratio and increases in the 1 : 3 blend ratio.

Prior to annealing, there is an increase of the fill factor with increasing PCBM concentration going from 1 : 1 to 1 : 2 ratio. Further increase to 1 : 3 ratio brings virtually no changes as compared to 1 : 2 ratio. The annealing process led to a decrease of FF in the 1 : 1 ratio, but an increase in the 1 : 2 and 1 : 3 ratios.

The trend in the J_{SC} and FF in these devices showed that with low PCBM concentration, the solar cells perform better before annealing, but with higher PCBM concentration better performance is achieved after annealing. The best performance was achieved with 1 : 2 blend ratio where V_{OC}, J_{SC} and FF values are relatively higher and stable even after annealing of the solar cells. The AFM images of these proportions (see below and Fig. S4†) also confirmed that there is no significant difference in morphology before and after annealing.

As can be seen from the IPCE curves in Fig. 6, a contribution to photocurrent from the absorption of PCBM is observed at a peak around 390 nm and a kink around 710 nm. This is evidenced from the intense optical absorption peak of the blend at around 390 nm, but not in the pure polymer film. The intensity of the IPCE peaks at 390 nm and 710 nm increased with increasing PCBM concentration. The IPCE of the solar cells increases from 1 : 1 to 1 : 2 polymer:PCBM blend ratio because the charge transport becomes more efficient with increasing PCBM amount[42] but the IPCE decreases as the amount of PCBM further increases in the 1 : 3 ratio (see also Fig. S2 and S3†). This is associated with the less contribution of PCBM to the total absorption in the visible spectral range leading to a decrease of the fraction of photons absorbed by the solar cell.[43] Integrating the IPCE data of the best cell measured after annealing in this experiment with **AnE-PV*stat***:PCBM 1 : 2 gives an estimate for J_{SC} under AM1.5 conditions of 7.80 mA cm^{-2} which is consistent with the J_{SC} value of 7.80 mA cm^{-2} obtained during *I–V* measurement. The slight difference observed in the nonannealed case between the calculated current from the IPCE (7.80 mA cm^{-2}) and the experimental value from the *I–V* measurement (7.82 mA cm^{-2}) lies within the range of error.

In summary high performance solar cells are obtained with **AnE-PV*stat*** even at low PCBM content as compared to those with lower $d_{\pi-\pi}$ values. In all 3 blending ratios efficiencies above 3% were achieved, whereby the best cell with **AnE-PV*stat***:PCBM (1 : 2) showed a V_{OC} of 830 mV, J_{SC} of 7.80 mA, a filling factor of 58% and an energy conversion efficiency of ~3.8%. Table 4 shows the consistency of the PV parameters.

The AFM surface morphology images of **AnE-PV*stat***:PCBM thin films with three different **AnE-PV*stat*** to PCBM ratios are presented in Fig. S4†. The top row of the figure shows the AFM images of as deposited films, while the bottom row shows the images of **AnE-PV*stat***:PCBM films annealed in an inert atmosphere at 110 °C for 5 minutes. The **AnE-PV*stat***:PCBM films with a 1 : 1 blend ratio show very smooth and almost featureless surfaces. Beside a slight increase of the surface roughness from 0.7 nm to 1.1 nm, no significant change is observed upon annealing (see Fig. S4a and S4b†). On the other hand, a well defined grain morphology is observed for the 1 : 2 blend ratio (see Fig. S4c and S4d†). In this case, upon annealing the grain size slightly decreases and a more compact film is obtained, which is reflected in a decrease of the surface roughness from around 4 nm to 2 nm. An additional increase of PCBM concentration from 1 : 2 to 1 : 3 blend ratio induces a further increase in the grain size, as observed in images Fig. S4e and S4f† in comparison with images Fig. S4c and S4d†. After annealing, the 1 : 3 ratio **AnE-PV*stat***:PCBM films become also slightly more compact and the surface roughness decreases from 6 to 4 nm.

It can be summarized that, for the ratios of PCBM, equal to (1 : 2) and (1 : 3), annealing of the blends resulted in more compact nature of the films which decreases the phase separation as evidenced from the decrease in surface roughness, explaining the enhancement of the solar cell performance observed in both cases, whereby the best performance was achieved for the 1 : 2 case due to optimal phase separation, as evidenced by the AFM morphology images.

By reducing the active layer thickness to about ~100 nm,[12] it was possible to achieve a power conversion efficiency of ~3.8% already with a 1 : 1 polymer:PCBM blend ratio. Similar improvement of the solar cell performance upon decrease of the active layer film thickness was observed in the past with

Table 5 Photovoltaic parameters of solar cells of polymer:PCBM for 1 : 1 and 1 : 2 blend ratios for **AnE-PV*ad***, **-*ab***, and **-*stat***. The active layer film thickness was ~100 nm.[12]

AnE-PV*i*:PCBM (blend ratio)	V_{OC}/mV	J_{sc}/mA cm^{-2}	FF (%)	η (%)
ad:PCBM (1 : 1)	650	5.66	41.33	1.52
ad:PCBM (1 : 2)	680	6.75	48.37	2.22
ab:PCBM (1 : 1)	810	6.13	49.08	2.44
ab:PCBM (1 : 2)	790	7.14	55.65	3.14
ba:PCBM (1 : 1)	770	1.59	27.38	0.34
ba:PCBM (1 : 2)	930	3.44	34.67	1.11
bb:PCBM (1 : 1)	840	1.99	29.23	0.49
bb:PCBM (1 : 2)	830	4.22	34.8	1.22
stat:PCBM (1 : 1)	830	8.49	53.44	3.77
stat:PCBM (1 : 2)	800	7.89	58.45	3.69

PPE-PPV compounds acting as acceptor components in a polymer–polymer bulk heterojunction construct.[41] Based on these results, a comparison with the study in ref.12*b* is possible. It shows that there is an increase of solar cell performance with increasing $d_{\pi-\pi}$ (Table 5). Keeping the side chain volume fraction equal as in **AnE-PV*ab***, ***-ba***, ***-bb*** and ***-stat***, the V_{OC} shows no significant difference, but the short circuit current J_{SC} and the filling factor FF depend on degree of stacking. No stacking ability at all as in the amorphous compounds **AnE-PV*ba*** and ***-bb*** favors very high miscibility between donor and acceptor, which in turn favors charge recombination and thus negatively affects the FF and J_{SC}. An increase in $d_{\pi-\pi}$, as observed from **AnE-PV*ab*** to ***-stat***, seems to positively affect J_{SC} and FF, and thus the overall performance. Fig. S5† depicts the *I–V* curves of the 1 : 1 and 1 : 2 polymer:PCBM blend ratios for the lower active layer film thickness.

In summary, **AnE-PV*stat*** is so far the best **AnE-PV** compound for solar cell application because of favorable side chains distribution.

Conclusion

The randomly grafting of segments of *linear octyloxy* and segments of *branched 2-ethylhexyloxy* side chains has resulted in a side chain based statistical copolymer **AnE-PV*stat*** showing far better features than its side chain based well defined congeners. As a consequence, relatively high (5.4×10^{-4} cm^2 V^{-1} s^{-1}) as well as electric field independent charge carrier mobility was measured by both CELIV and OFET techniques. The ***-stat*** hole mobility values are close to those of the amorphous polymers ***-ba*** and ***-bb***, leading to the conclusion that charge carrier mobility is more an *intra*chain process than an *inter*chain one, in agreement with past photoconductivity results carried out with PPE-PPVs.[38] The present state-of–art efficiency of ~3.8% for PPV based materials has been achieved for **AnE-PV*stat*** even at fullerene contents of 50% for thinner active layer films. For thicker films, annealing step at 110 °C was necessary to enhance the solar cell performance for 1 : 2 and 1 : 3 **AnE-PV*stat***:PCBM blend ratios.

Acknowledgements

Daniel A. M. Egbe, and Harald Hoppe are grateful to the DFG (*Deutsche Forschungsgemeinschaft*) for financial support in the framework of SPP1355. Vera Cimrova acknowledges the support of the Ministry of Education, Youth and Sports of the Czech Republic (grant No.1M06031), Alberto M. Ramil is grateful for financial support through project FWF/NFN S 9711-N20.

References

1 N. S. Sariciftci, L. Smilowitz, A. J. Heeger and F. Wudl, *Science*, 1992, **258**, 1474.
2 (*a*) H. Hoppe and N. S. Sariciftci, *Adv. Polym. Sci.*, 2008, **214**, 1; (*b*) S. Günes, H. Neugebauer and N. S. Sariciftci., *Chem. Rev.*, 2007, **107**, 1324; (*c*) G. Dennler, C. Lungenschmied, H. Neugebauer, N. S. Sariciftci and A. Labouret, *J. Mater. Res.*, 2005, **20**, 3224; (*d*) Y.-J. Cheng, S.-H. Yang and C.-S. Hsu, *Chem. Rev.*, 2009, **109**, 5868.
3 (*a*) C. J. Brabec, J. A. Hauch, P. Schilinsky and C. Waldauf, *MRS Bull.*, 2005, **30**, 50; (*b*) G. Li, V. Shotriya, J. Huang, Y. Yao, T. Moriarty, K. Emery and Y. Yang, *Nat. Mater.*, 2005, **4**, 864.
4 (*a*) W. Ma, C. Yang, X. Gong, K. Lee and A. J. Heeger, *Adv. Funct. Mater.*, 2005, **15**, 1617; (*b*) M. Reyes-Reyes, K. Kim and D. L. Carolla, *Appl. Phys. Lett.*, 2005, **87**, 083506.
5 I. McCulloch, M. Heeney, M. L. Chabinyc, D. DeLongchamp, R. J. Kline, M. Cölle, W. Duffy, D. Fischer, D. Gundlach, B. Hamadani, R. Hamilton, L. Richter, A. Salleo, M. Shkunov, D. Sparrowe, S. Tierney and W. Zhang, *Adv. Mater.*, 2009, **21**, 1091.
6 (*a*) J. Y. Kim, K. Lee, N. S. Coates, D. Moses, T. Q. Nguyen, M. Dante and A. J. Heeger, *Science*, 2007, **317**, 222; (*b*) S. H. Park, A. Roy, S. Beaupre, S. Cho, N. Coates, J. S. Moon, D. Moses, M. Leclerc, K. Lee and A. J. Heeger, *Nat. Photonics*, 2009, **3**, 297.
7 (*a*) H.-Y. Chen, J. Hou, S. Zhang, Y. Liang, G. Yang, Y. Yang, L. Yu, Y. Wu and G. Li, *Nat. Photonics*, 2009, **3**, 649; (*b*) Y. Liang, D. Feng, Y. Wu, S.-T. Tsai, G. Li, C. Ray and L. Yu, *J. Am. Chem. Soc.*, 2009, **131**, 7792.
8 http://www.neubers.de/Solar-Taschen.
9 H. Hoppe and N. S. Sariciftci, *J. Mater. Chem.*, 2006, **16**, 45.
10 (*a*) Y. Yao, J. Hou, Z. Xu, G. Li and Y. Yang, *Adv. Funct. Mater.*, 2008, **18**, 178; (*b*) L. Chen, Z. Hong, G. Li and Y. Yang, *Adv. Mater.*, 2009, **21**, 1434.
11 (*a*) D. A. M. Egbe, L. H. Nguyen, H. Hoppe, D. Mühlbacher and N. S. Sariciftci, *Macromol. Rapid Commun.*, 2005, **26**, 1389; (*b*) D. A. M. Egbe, L. H. Nguyen, K. Schmidtke, A. Wild, C. Sieber, S. Guenes and N. S. Sariciftci, *J. Polym. Sci., Part A: Polym. Chem.*, 2007, **45**, 1619; (*c*) D. A. M. Egbe, B. Carbonnier, E. Birckner and U.-W. Grummt, *Prog. Polym. Sci.*, 2009, **34**, 1023.
12 (*a*) R. Jadhav, S. Türk, F. Kühnlenz, V. Cimrova, S. Rathgeber, D. A. M. Egbe and H. Hoppe, *Phys. Status Solidi A*, 2009, **12**, 2695; (*b*) D. A. M. Egbe, S. Türk, S. Rathgeber, F. Kühnlenz, R. Jadhav, A. Wild, E. Birckner, G. Adam, A. Pivrikas, V. Cimrova, G. Knör, N. S. Sariciftci and H. Hoppe, *Macromolecules*, 2010, **43**, 1261.
13 S. Rathgeber, D. Bastos de Toledo, E. Birckner, H. Hoppe and D. A. M. Egbe, *Macromolecules*, 2010, **43**, 306.
14 D. T. McQuade, A. E. Pullen and T. M. Swager, *Chem. Rev.*, 2000, **100**, 2537.
15 A. J. J. M. van Breemen, P. T. Herwig, C. H. T. Chlon, J. Sweelssen, H. F. M. Schoo, E. M. Benito, D. M. de Leeuw, C. Tanase, J. Wildeman and P. W. M. Blom, *Adv. Funct. Mater.*, 2005, **15**, 872.
16 Y. Zhang, K. Tajima, K. Hirota and K. Hashimoto, *J. Am. Chem. Soc.*, 2008, **130**, 7812.
17 A. Wild, D. A. M. Egbe, E. Birckner, V. Cimrova, R. Baumann, U.-W. Grummt and U. S. Schubert, *J. Polym. Sci., Part A: Polym. Chem.*, 2009, **47**, 2243.
18 G. Juška, K. Arlauskas and M. Viliunas, *Phys. Rev. Lett.*, 2000, **84**, 4946.
19 G. Dennler, A. J. Mozer, G. Juška, A. Pivrikas, R. Österbacka, A. Fuchsbauer and N. S. Sariciftci, *Org. Electron.*, 2006, **7**, 229.
20 R. Österbacka, A. Pivrikas, G. Juška, K. Genevicius, K. Arlauskas and H. Stubb, *Curr. Appl. Phys.*, 2004, **4**, 534.
21 D. A. M. Egbe, E. Tekin, E. Birckner, A. Pivrikas, N. S. Sariciftci and U. S. Schubert, *Macromolecules*, 2007, **40**, 7786.
22 A. Palmaerts, L. Lutsen, T. J. Cleij, D. Vanderzande, A. Pivrikas, H. Neugebauer and N. S. Sariciftci, *Polymer*, 2009, **50**, 5007.
23 A. J. Mozer, N. S. Sariciftci, A. Pivrikas, R. Österbacka, G. Juška, L. Brassat and H. Bässler, *Phys. Rev. B: Condens. Matter*, 2005, **71**, 035214.
24 A. J. Mozer, G. Dennler, N. S. Sariciftci, M. Westerling, A. Pivrikas, R. Österbacka and G. Juška, *Phys. Rev. B: Condens. Matter*, 2005, **72**, 035217.
25 A. Pivrikas, N. S. Sariciftci, G. Juska and R. Österbacka, *Prog. Photovoltaics*, 2007, **15**, 677.
26 A. Pivrikas, P. Stadler, H. Neugebauer and N. S. Sariciftci, *Org. Electron.*, 2008, **9**, 775.
27 G. Juska, K. Genevicius, K. Arlauskas, R. Österbacka and H. Stubb, *Phys. Rev. B: Condens. Matter*, 2002, **65**, 233208.
28 T. Moehl, V. G. Kytin, J. Bisquert, M. Kunst, H. J. Bolink and G. Belmonte, *ChemSusChem*, 2009, **2**, 314.
29 H. Horowitz, R. Hailaoui, R. Bourguiga and M. Hailaoui, *Synth. Met.*, 1999, **101**, 401.
30 S. M. Sze and K. N. Kwok, *Physics of Semiconductor Devices*, John Wiley & Sons, Inc., Hoboken, New Jersey, 3rd edn, 2007.

31 G. Horowitz, *J. Mater. Res.*, 2004, **19**, 1946.
32 G. Horowitz, R. Hailaoui, R. Bourguiga and M. Hailaoui, *Synth. Met.*, 1999, **101**, 401.
33 D. Braga and G. Horowitz, *Adv. Mater.*, 2009, **21**, 1.
34 F. Dinelli, M. Murgia, P. Levy, M. Cavallini, F. Biscarini and D. M. de Leeuw, *Phys. Rev. Lett.*, 2004, **92**, 116802.
35 A. Pivrikas, R. Österbacka, G. Juska, K. Arlauskas and H. Stubb, *Synth. Met.*, 2005, **155**, 242.
36 H. Bässler, *Phys. Status Solidi B*, 1993, **175**, 15.
37 C. R. Newman, C. D. Frisbie, D. A. da Silva Filho, J.-L. Brédas, P. C. Ewbank and K. R. Mann, *Chem. Mater.*, 2004, **16**, 4436.
38 (*a*) D. A. M. Egbe, C. P. Roll, E. Birckner, U.-W. Grummt, R. Stockmann and E. Klemm, *Macromolecules*, 2002, **35**, 3825; (*b*) D. A. M. Egbe, C. Bader, J. Nowotny, W. Günther and E. Klemm, *Macromolecules*, 2003, **36**, 5459; (*c*) D. A. M. Egbe, C. Bader, E. Klemm, L. Ding, F. Karasz, U.-W. Grummt and E. Birckner, *Macromolecules*, 2003, **36**, 9303.
39 Y.-K. Lan, C.-H. Yang and H.-C. Yang, *Polym. Int.*, 2010, **59**, 16.
40 G. Yu and A. J. Heeger, *J. Appl. Phys.*, 1995, **78**, 4510.
41 T. Kietzke, D. A. M. Egbe, H.-H. Hörhold and D. Neher, *Macromolecules*, 2006, **39**, 4018.
42 S. Günes, A. Wild, E. Cevik, A. Pivrikas, U. S. Schubert and D. A. M. Egbe, *Sol. Energy Mater. Sol. Cells*, 2010, **94**, 484.
43 C. J. Brabec, A. Cravino, D. Meissner, N. S. Sariciftci, T. Fromherz, M. Minse, L. Sanchez and J. C. Hummelen, *Adv. Funct. Mater.*, 2001, **11**, 374.

